# Chapter 5
# Measurement Methods for Critical Current Density

## 5.1 Four Terminal Method

The most general method for measuring the critical current density $J_c$, an important parameter of superconductors, is the four terminal method, in which the voltage drop $V$ between the terminals is measured as a function of the transport current $I$. This is also called the resistive method. The critical current $I_c$ is defined as the transport current at which the flow voltage clearly appears. The critical current density is given by $I_c$ divided by the cross-sectional area $S$ of the superconducting region: $J_c = I_c/S$. In multi-filamentary superconductors, the cross-sectional area may include a metallic stabilizer and reinforcing materials.

In practice, the current-voltage curves of superconducting wires are not straight lines as in Fig. 1.13 due to various causes such as inhomogeneity of the critical current density or the effect of flux creep described in Sect. 3.8. Instead, voltage gradually rises due to various causes, which will be described later. The measurement is also subject to sensitivity limits. Hence, there is no clear point at which the flow voltage appears. To define the critical current, the following criteria are used.

(1) *Electric field criterion*: This is the simplest method. The critical current is defined by the current at which the electric field reaches a certain value (see Fig. 5.1). A value of 100 $\mu V\,m^{-1}$ or 10 $\mu V\,m^{-1}$ is commonly used.
(2) *Resistivity criterion*: The critical current is defined by the current at which the resistivity of the superconducting wire reaches a certain value (see Fig. 5.1). For composite superconductors with stabilizer, $10^{-13}\ \Omega\,m$ or $10^{-14}\ \Omega\,m$ is commonly used.
(3) *Off-set method*: The critical current is determined by the current at which a tangential line from part of the current-voltage curve crosses zero voltage (see Fig. 5.1).

A large error results from the electric field criterion and the resistivity criterion when flux creep is pronounced. Even in the case where the current-voltage curve shows an ohmic characteristic as in (3.132), a nonzero critical current density is defined using the electric field criterion. Similar thing happens also when the

T. Matsushita, *Flux Pinning in Superconductors*,
Springer Series in Solid-State Sciences 178,
DOI 10.1007/978-3-642-45312-0_5, 

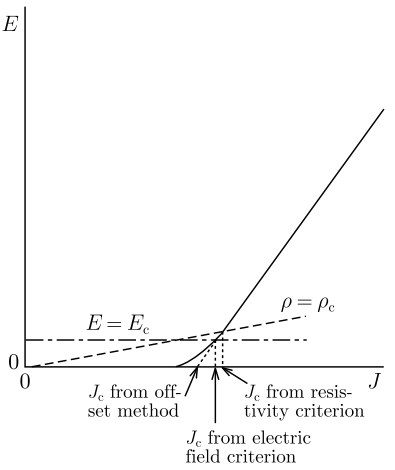


**Fig. 5.1** Current-voltage curve and methods of determination of critical current density using respective criteria

resistivity criterion is used. These methods are useful only for a strongly nonlinear current-voltage curve, which rises abruptly at a nonzero current density. If the current-voltage curve is expressed as

$$V \propto I^n, \tag{5.1}$$

the index, $n$, is called the $n$ value. The $n$ value is a supplementary parameter representing the strength of the nonlinearity. The electric field range of 1 $\mu V\,m^{-1}$ to 100 $\mu V\,m^{-1}$ is generally used to determine the $n$ value. A superconducting wire with larger $n$ is often better. Note that it is possible to reduce the induced voltage drastically by reducing the current slightly when $n$ is high. When $n$ is low, on the other hand, the induced voltage does not become small abruptly when the current is decreased slightly. To avoid errors when $n$ is small, it is practical to use the offset method. Using the line tangent to the curve at the current density at the electric field criterion $J_0$, the critical current density determined by the offset method is

$$J_c' = \left(1 - \frac{1}{n}\right) J_0. \tag{5.2}$$

This gives the correct result $J = 0$ for $n = 1$.

Here the meaning of the $n$ value is discussed. The current-voltage characteristics deviate from (2.31), the relationship of which is shown in Fig. 1.13, and the voltage rises gradually near $J_c$. This voltage is due to both microscopic causes, such as flux creep and the nonlinearity of flux motion around the pinning potential, and macroscopic causes such as spatial nonuniformity of the critical current density and sausaging of superconducting filaments. Sausaging is a nonuniformity of the filament diameter as a result of wire drawing. Therefore, it is difficult to derive an $n$ value directly as a physical quantity; the $n$ value is merely a convenient parameter for practical use.

If the dispersion of $J_c$ originates from the dispersion of $T_c$, its value $\Delta J_c$ does not vary appreciably even at high temperatures and high magnetic fields. Thus, $\Delta J_c / J_c$

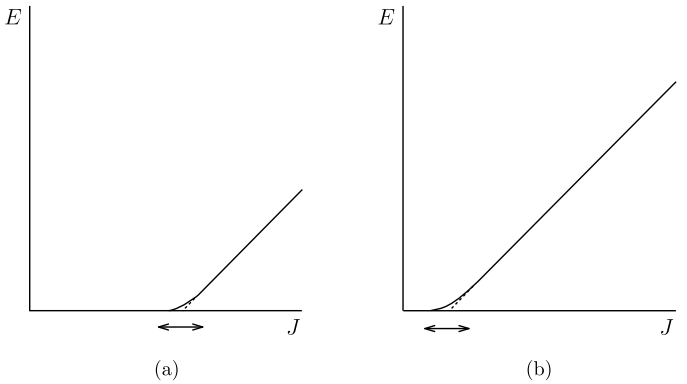


**Fig. 5.2** Current-voltage curves at (**a**) low temperatures and/or low magnetic fields and (**b**) high temperatures and/or high magnetic fields. Arrows show ranges of distribution of critical current density. At high temperatures and/or high magnetic fields, the deviation is relatively large in comparison with the mean value of the critical current density, and the $n$ value is small

is larger at higher temperatures and at higher magnetic fields as shown in Fig. 5.2. In addition, the effect of flux creep becomes pronounced under these circumstances. Hence, the $n$ value is a decreasing function of $T$ and $B$.

Equation (5.1) insists that a true superconducting state with zero resistivity does not exist. The flux creep theory predicts that the electric field abruptly decreases exponentially in a region of ultra low electric field, far below the sensitivity of present measuring techniques. However, the electric field is not zero even in this case. This is associated with the fact that the state in which the flux lines are pinned by pinning potentials is not at equilibrium. Hence, the process of relaxation to the equilibrium state with zero current density cannot be avoided. Shortly after the discovery of high-temperature superconductors, many researchers thought that these superconductors could not be applied to the field of technology. Although the above properties are true, it is not true that these superconductors cannot be applied.

Assume that (5.1) applies approximately within some range of current. When the current is reduced by a factor $p$, the voltage can be reduced by a factor $p^n$. Hence, if the loss associated with the voltage drop can be reduced below that of an equivalent nonsuperconducting metal by reducing the current by an appropriate factor, practical application of the superconductor can be realized. For example, consider a superconducting coil that is made of 1 km of wire with a critical current of 200 A at the electric field criterion of 100 $\mu V\,m^{-1}$. When this coil is driven at the critical current, the voltage is 0.1 V and the loss power is 20 W. However, if the $n$ value of the wire is 50, the loss power is reduced to 0.5 W by reducing the current to $0.93I_c$. This power may be much less than the heat transmitted into a cryostat. Thus, the coil can be applied as a superconducting device. As demonstrated by this example, if the $n$ value is sufficiently large, even a relatively weak electric field criterion such as 100 $\mu V\,m^{-1}$ can be used to define $I_c$. The $n$ value in commercial superconducting wires exceeds 50, and $n = 21$ has been reported [1] for a Bi-2223 tape at 77.3 K in the self field.

## 5.2 DC Magnetization Method

The DC magnetization of a superconductor is hysteretic as mentioned in Sect. 2.5. Consider a superconducting slab with thickness $2d$. In low magnetic fields, the field dependence of the pinning force density can be approximated by (2.46). Then, the parameters $\alpha_c$ and $\gamma$ are determined such that (2.55a)–(2.55e) fits an observed magnetization curve, and the local critical current density can be obtained from $\alpha_c \hat{B}^{\gamma-1}$ (see (2.50)).

If the magnetization contains a diamagnetic component as mentioned in Sect. 2.6, this contribution should be eliminated. This is possible only when the diamagnetic property is known. However, even if the property is unknown, the diamagnetic effect can be approximately canceled out in the hysteresis of magnetization between increasing and decreasing fields. This is a good approximation for superconductors with a large G-L parameter $\kappa$.

The hysteresis of magnetization of a superconducting slab in a parallel external $H_e$ is calculated from (2.55b) and (2.55d):

$$\Delta M = \frac{2-\gamma}{3-\gamma} H_p \left\{ \left[ \left( \frac{H_e}{H_p} \right)^{2-\gamma} + 1 \right]^{(3-\gamma)/(2-\gamma)} + \left[ \left( \frac{H_e}{H_p} \right)^{2-\gamma} - 1 \right]^{(3-\gamma)/(2-\gamma)} - 2 \left( \frac{H_e}{H_p} \right)^{3-\gamma} \right\}. \tag{5.3}$$

The parameters $\alpha_c$ and $\gamma$ can be estimated by fitting the observed hysteresis to the above theoretical result. By contrast, the critical current density obtained by the transport method is a spatial average of the local critical current density (see Sect. 2.5).

The average magnetic critical current density is usually estimated from

$$J_c = \frac{\Delta M}{d}. \tag{5.4}$$

This is correct only when the local critical current density is constant throughout the sample, i.e., when the Bean-London model holds.

The average transport critical current density $\langle J_c \rangle$ at external magnetic field $H_e$ is given by (2.61). $\langle J_c \rangle$ can also be obtained from $\Delta M$. The solid lines in Fig. 5.3 show the magnetic flux distributions in the processes of increasing and decreasing the magnetic field, and the area of the diamond-shaped region is equal to $2\mu_0 \Delta M d$. The broken line in the figure is the flux distribution when the transport current reaches the critical value in the external field $H_e$. When the external magnetic field is sufficiently larger than the penetration field $H_p$, (5.3) reduces to

$$\Delta M \simeq \frac{H_p}{2-\gamma} \left( \frac{H_p}{H_e} \right)^{1-\gamma} \left[ 1 + \frac{(1-\gamma)(3-2\gamma)}{12(2-\gamma)^2} \left( \frac{H_p}{H_e} \right)^{4-2\gamma} \right]. \tag{5.5}$$

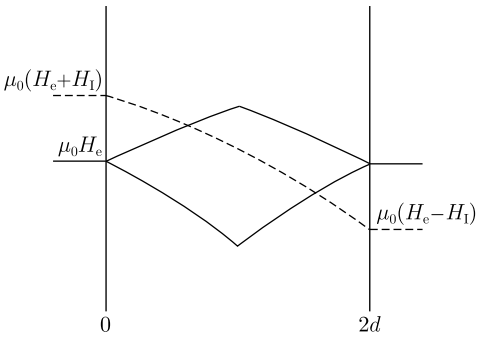


**Fig. 5.3** Magnetic flux distributions in a superconducting slab during a magnetization measurement (*solid lines*) and that in the critical state during a transport measurement (*broken line*). $H_I$ represents the self field of the current

Thus, in terms of $\Delta M$, $\langle J_c \rangle$ is given by

$$\langle J_c \rangle \simeq \frac{\Delta M}{d}\left[1 + \frac{(1-\gamma)(4\gamma-3)}{12}\left(\frac{\Delta M}{H_e}\right)^2\right]. \tag{5.6}$$

The second term gives the correction to (5.4). This is very small when the external field is large. In the case where $\gamma = 0.5$ and $H_e = 2H_p$, the second term gives a correction of about 0.2 %.

## 5.3 Campbell's Method

The shielding current density induced in the superconductor by an AC magnetic field can be estimated by measuring the penetrating flux. One method is Campbell's method [2], explained in this section. By using this method, not only the current density but also the relationship between the force on and the displacement of the flux lines can be derived. The analysis of the force-displacement profile is useful for investigating the reversible motion of flux lines described in Sect. 3.7 and the flux pinning properties described in Chap. 7. Other AC inductive methods will be introduced in Sect. 5.4.

Usually a DC magnetic field $H_e$ and a small AC field $h_0 \cos \omega t$ are applied parallel to a superconducting cylinder or long slab, as shown in Fig. 5.4, to avoid the

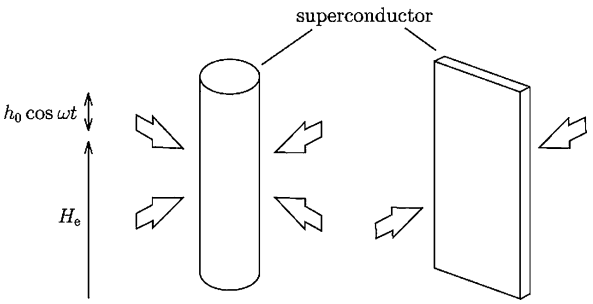


**Fig. 5.4** Application of magnetic field commonly used in Campbell's method. *Arrows* show the directions of penetration of AC magnetic flux

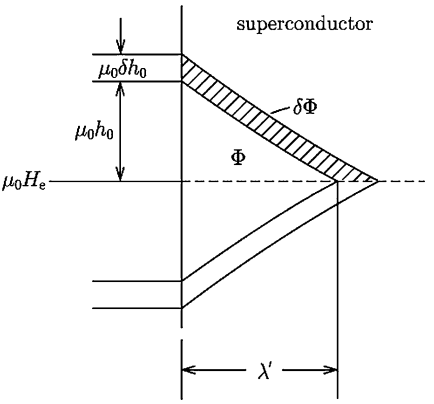


**Fig. 5.5** Variation in penetration of AC magnetic flux when the AC field amplitude is slightly changed from $h_0$ to $h_0 + \delta h_0$. Current density is assumed to be constant

effect of demagnetization due to the specimen shape. The magnetic flux moving into and out of the specimen is measured using a pick-up coil and a reference coil. The amplitude of penetrating flux is denoted by $\Phi$, and $\delta\Phi$ corresponds to the incremental flux change when $h_0$ is slightly increased by $\delta h_0$. The magnetic flux distribution is expected to be like the one shown in Fig. 5.5. The shielding current density, which is not necessarily equal to the critical value, is considered to be unchanged when the AC field amplitude increases from $h_0$ to $h_0 + \delta h_0$. Then, the depth of penetration of the AC field is given by

$$\lambda' = \frac{1}{2w\mu_0} \cdot \frac{\delta\Phi}{\delta h_0} \tag{5.7}$$

when the width $w$ of the slab specimen is much larger than the thickness $2d$. In a strict sense, $2w$ in the denominator of (5.7) is replaced by the perimeter of the superconducting slab $2(w + 2d)$, when $\lambda'$ is sufficiently smaller than $2d$. In the limit of small $\delta h_0$, $\delta\Phi/\delta h_0$ reduces to the derivative, $\partial\Phi/\partial h_0$. Then, (5.7) leads to

$$\lambda' = \frac{1}{2w\mu_0} \cdot \frac{\partial\Phi}{\partial h_0}. \tag{5.8}$$

In a cylindrical superconductor with radius $R$, a simple calculation gives

$$\lambda' = R\left[1 - \left(1 - \frac{1}{\pi R^2\mu_0} \cdot \frac{\partial\Phi}{\partial h_0}\right)^{1/2}\right]. \tag{5.9}$$

When $\lambda' \ll R$, the right-hand side of (5.9) reduces to $(2\pi R\mu_0)^{-1}\partial\Phi/\partial h_0$. This result is understandable from the fact that the perimeter is equal to $2\pi R$. The derivative of $\Phi$ with respect to $h_0$ in (5.8) and (5.9) can be obtained by expressing $\Phi$ as a polynomial of $h_0$.

An example of $\lambda'(h_0)$ is shown in Fig. 5.6 [3]. Except for small $h_0$, this $\lambda'$-$h_0$ characteristic can be regarded as the flux distribution in the superconductor for increasing field; the ordinate and abscissa represent the internal magnetic flux density

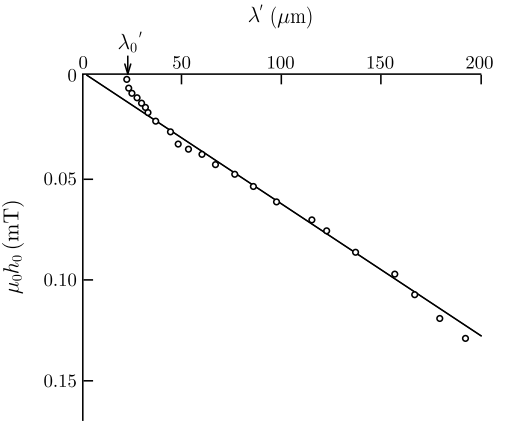


**Fig. 5.6** Example of measurement of the $\lambda'$ vs. $h_0$ characteristics using a modified Campbell's method for Nb-50at%Ta at $\mu_0 H_e = 0.336$ T [3]. The prediction of the Bean-London model holds except in the region of small $h_0$

and the depth of flux penetration, respectively. Hence, the slope of this distribution gives $\mu_0 J$:

$$J = \left( \frac{\partial \lambda'}{\partial h_0} \right)^{-1}. \tag{5.10}$$

which is equal to $J_c$ in the critical state. In Fig. 5.6 it is found that the prediction of the Bean-London model is satisfied. Derivation of the magnetic flux distribution and the critical current density is requested in Exercise 5.1 using (5.8) and (5.9) for the Bean-London model. Note that the penetration depth $\lambda'$ is finite, $\lambda' = \lambda'_0$, deviating from the Bean-London model, when $h_0$ is small. This value ($\lambda'_0$) is Campbell's AC penetration depth, given by (3.93). In this region the reversible motion of flux lines mentioned in Sect. 3.7 is pronounced, and the apparent magnetic flux distribution in Fig. 5.6 is different from the real one. That is, although (5.10) predicts a large current density, this may not be correct. The real distribution is like the one shown in Fig. 3.33(a), and the current density takes a reasonable value. In this region the penetrating flux is approximately given by (3.92), and a replacement of $b(0)$ by $\mu_0 h_0$ gives

$$\Phi \simeq 2w \int_0^\infty \mu_0 h_0 \exp\left( -\frac{x}{\lambda'_0} \right) \mathrm{d}x = 2w \mu_0 h_0 \lambda'_0 \tag{5.11}$$

for a superconducting slab sufficiently thicker than $\lambda'_0$. Substitution of this into (5.8) leads to

$$\lambda' = \lambda'_0, \tag{5.12}$$

which coincides with experiment.

In Campbell's method [2] the amplitude of penetrating AC flux $\Phi$, i.e., half of the difference between the magnetic flux at $\omega t = -\pi$ and that at $\omega t = 0$ is measured. There is also a similar method [4], in which a fundamental frequency component of the AC flux $\Phi'$ is approximately measured instead of $\Phi'$, followed by the same analysis. The resultant error due to this approximation is estimated in Exercise 5.2.

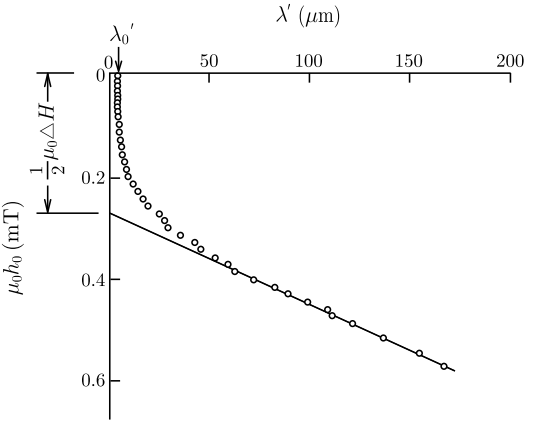


**Fig. 5.7** Example of measurement of the $\lambda'$ vs. $h_0$ characteristics using the modified Campbell's method for Nb-50at%Ta, the same specimen as that in Fig. 5.6, but at $\mu_0 H_e = 0.123$ T [6]. Extrapolation of the linear part does not go through the origin, and is thus different from Fig. 5.6. This shows a strong flux pinning near the surface

In another method [5], instantaneous values of the external AC field and penetrating AC flux, represented by $h(t)$ and $\Phi(t)$, are measured. Since the relationship between these quantities is the same as that between $h_0$ and $\Phi$, $(\partial\Phi(t)/\partial t)/(\partial h(t)/\partial t)$ is equal to $\partial\Phi/\partial h_0$. Thus, (5.8) can be rewritten as

$$\lambda' = \frac{1}{2w\mu_0} \cdot \frac{\partial\Phi(t)/\partial t}{\partial h(t)/\partial t}. \tag{5.13}$$

The denominator $(\mu_0 \partial h(t)/\partial t)$ and the numerator $(\partial\Phi(t)/\partial t)$ are the voltages measured directly by a field monitor coil and a pick-up coil, respectively. This is the wave-form analysis method. A characteristic of this method is that differentiation as in (5.8) is not necessary.

In such AC inductive methods, many more measurements and analyses are needed to determine $J_c$ than in the four terminal method and the DC magnetization method. However, other important information can also be obtained. One of them is the relationship between the pinning force and the displacement of flux lines, which will be discussed later. Observation of an inhomogeneous current distribution is also possible, although applicable cases are limited. Figure 5.7 shows an example of an observed flux distribution using a modified Campbell's method for a specimen with a surface irreversibility, [6] which is discussed in Sect. 3.5. While the flux distribution is linear with a uniform critical current density in the inner region, its extrapolation does not pass through the origin, suggesting that a large magnetization is caused by a high density of shielding current flowing in the surface region. This analysis will be described later. When the shielding current flows in an inhomogeneous way, depending on a depth from the surface, as in the case of surface irreversibility, such an inhomogeneous current distribution, which cannot be obtained by the four terminal method and the DC magnetization method, can be obtained by this method. However, observable quantities are those averaged along the direction normal to the flux penetration, so any inhomogeneity along this direction cannot be obtained. Another example is the simultaneous observation of intra-and

inter-grain critical current densities in sintered Y-based oxide superconductors with weakly coupled grains [7].

According to the analysis in [8], the relationship between the pinning force density $F$ and the displacement of flux lines $u$ is derived as follows. The equations used for this analysis are (3.89), the continuity equation for flux lines:

$$\frac{\mathrm{d}u}{\mathrm{d}x} = -\frac{b}{\mu_0 H_\mathrm{e}} \tag{5.14}$$

and the force-balance equation between the Lorentz force $F_\mathrm{L}$ and the pinning force density $F$ (see (3.90)):

$$-F = F_\mathrm{L} = -H_\mathrm{e}\frac{\mathrm{d}b}{\mathrm{d}x} + \text{const.} \tag{5.15}$$

Note that this gives the absolute Lorentz force density, being different from (3.90), and the constant term on the right side is the value in the initial state ($b = 0$). The displacement of flux lines at the superconductor surface is initially obtained from (5.14). The AC field amplitude is denoted by $h_0$. The displacement in the half cycle from $\omega t = -\pi$ (the initial state) to $\omega t = 0$ is positive, suggesting that flux lines move along the direction of the positive $x$-axis. This can be expressed in terms of the amplitude of observed magnetic flux $\Phi$ as

$$u(0) = -\frac{1}{\mu_0 H_\mathrm{e}}\int_d^0 b(x)\mathrm{d}x = \frac{\Phi}{\mu_0 H_\mathrm{e} w}. \tag{5.16}$$

Assume that the initial state is the critical state with $F_\mathrm{L} = -\mu_0 J_\mathrm{c} H_\mathrm{e}$, as is satisfied in many experiments. Then, the pinning force density on flux lines at the surface is given by

$$-F = F_\mathrm{L} = -H_\mathrm{e}\left(\frac{\partial b}{\partial u}\cdot\frac{\partial u}{\partial x}\right)_{x=0} - \mu_0 J_\mathrm{c} H_\mathrm{e}. \tag{5.17}$$

From (5.14) and the relationship $(\partial b/\partial u)_{x=0} = [\partial b(0)/\partial\Phi]\cdot[\partial\Phi/\partial u(0)] = \mu_0 H_\mathrm{e}/\lambda'$, the above equation reduces to

$$-F = \frac{2\mu_0 H_\mathrm{e} h_0}{\lambda'} - \mu_0 J_\mathrm{c} H_\mathrm{e}. \tag{5.18}$$

This quantity is also obtained from the observed result of $\lambda'$.

Thus, $-F$ and $u(0)$ are obtained from $\lambda'$ and $\Phi$ at each $h_0$, respectively. The force-displacement profile can be derived directly by plotting these results. Figure 5.8 shows the force-displacement profile for a Nb-Ta specimen [3], the magnetic flux distribution (the $\lambda'$ vs. $h_0$ characteristics) of which was shown in Fig. 5.6. While the pinning force density varies linearly with the displacement of flux lines for a small displacement, it reaches a constant value asymptotically in the opposite critical state when the displacement becomes large. The $J_\mathrm{c}$ obtained from the saturated pinning force density is naturally equal to $J_\mathrm{c}$ obtained from the magnetic flux distribution.

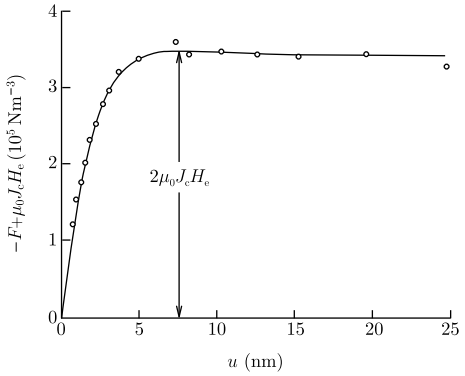


**Fig. 5.8** Pinning force density vs. displacement of flux lines [3], corresponding to the $\lambda'$ vs. $h_0$ characteristics in Fig. 5.6

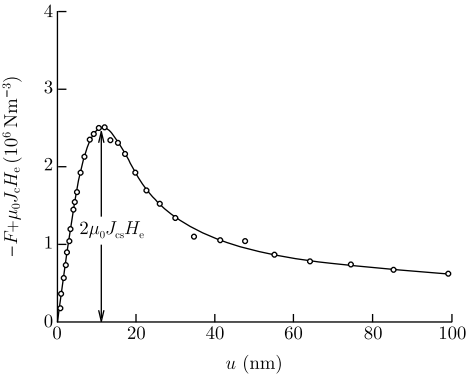


**Fig. 5.9** Pinning force density vs. displacement of flux lines [6], corresponding to the $\lambda'$ vs. $h_0$ characteristics in Fig. 5.7. A large peak of the pinning force density appears due to the strong surface pinning. $J_{cs}$ is the critical current density in the surface region

What will be the results of the same analysis in the case of significant surface irreversibility? Figure 5.9 is the force-displacement profile [6] corresponding to the magnetic flux distribution shown in Fig. 5.7, where the pinning force density initially increases with displacement, reaching a large peak, and then deceases gradually with increasing displacement. The peak of the pinning force density originates from the strong surface pinning, and the critical current density in the surface region can be estimated from the peak value. That is, if the peak value of the pinning force density measured from the initial state is denoted by $F_m$, the surface critical current density is given by $J_{cs} \simeq F_m/2\mu_0 H_e$. The surface critical current density shown in Fig. 3.26 was obtained by this method. When the displacement becomes sufficiently large as in Fig. 5.9, the pinning force density asymptotically approaches the bulk value.

Within the region of small displacement where the pinning force density varies linearly with the displacement, the motion of flux lines is limited inside the pinning potentials, and the phenomenon is almost reversible, as mentioned in Sect. 3.7. This linear relationship is represented by (3.88), and the coefficient $\alpha_L$, called the Labusch parameter, means the second spatial derivative of the averaged effective pinning potential. Hence, the pinning potential energy of flux lines in a unit volume

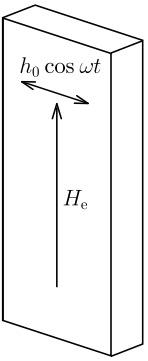


**Fig. 5.10** Manner of application of magnetic field when measuring the critical current density in a longitudinal magnetic field using the modified Campbell's method. Magnetic flux moving into and out of the specimen due to the AC magnetic field is measured

is given by

$$\hat{U}_0 = \frac{\alpha_L d_i^2}{2}. \tag{5.19}$$

Equation (3.95) holds for $\alpha_L$, $J_c$ and $d_i$, the interaction distance. Such information on the pinning potential can be obtained by using Campbell's methods. Thus, this method is useful for investigating electromagnetic phenomena. For example, since the pinning potential energy $U_0$ discussed in Sect. 3.8 is equal to $\hat{U}_0$ multiplied by the flux bundle volume, this volume can be estimated from $\hat{U}_0$ and $U_0$ obtained by an AC inductive method and by a measurement of irreversibility field, respectively. In other areas, the flux pinning mechanism is usually investigated by measuring the dependencies of the pinning force density on magnetic field and temperature (temperature scaling law), and on pinning parameters such as the elementary pinning force and the number density of defects (summation problem). Even in this case a more precise investigation is possible by measuring the dependencies of $\alpha_L$ or $d_i$ on these pinning parameters (see Sects. 7.5 and 8.2).

An evaluation of the critical current density in a longitudinal magnetic field, $J_{c\parallel}$, is also possible [9] by measuring the response of a superconducting slab to a transverse AC field superimposed on the longitudinal DC field as shown in Fig. 5.10. In this case the shielding current induced by the AC field is perpendicular to the AC field, and hence, parallel to the DC field. Figure 4.26 is an example of the distribution of the transverse magnetic flux obtained by this method.

An outline of the AC inductive methods such as Campbell's method was briefly given above. However, note that these methods are not always effective. For example, the method based on the irreversible critical state model does not allow correct results to be derived for superconducting specimens of a size comparable to or smaller than Campbell's AC penetration depth $\lambda_0'$ in which the reversible flux motion is pronounced (see Sect. 3.7). Consider the reason (Exercise 5.3). However, if the imaginary part of the complex susceptibility is measured over a wide range of AC field amplitude, the critical current density can be approximately estimated, as will be shown in the next section. On the other hand, one of the simple methods used to estimate the critical current density in such small specimens is a calculation from the hysteresis of a major DC magnetization curve.

## 5.4 Other AC Inductive Methods

### 5.4.1 Third Harmonic Analysis

The critical current density of a superconducting specimen can also be estimated by measuring the third harmonic voltage induced by an AC magnetic field [10]. For example, it is assumed that a DC field $H_e$ and an AC field $h_0 \cos \omega t$ are applied parallel to a wide superconducting slab of thickness $2d$ ($0 \le x \le 2d$). If the magnetic flux density averaged within the superconducting slab is expressed as

$$\langle B \rangle = h_0 \sum_{n=0}^{\infty} \mu_n \cos(n\omega t + \theta_n). \tag{5.20}$$

$\mu_n$ ($n \ge 2$) represents the harmonic components of the AC permeability. These components ($n \ge 1$) are given by

$$\mu_n = \left(\mu_n'^2 + \mu_n''^2\right)^{1/2}, \tag{5.21}$$

$$\mu_n' = \frac{1}{\pi h_0} \int_{-\pi}^{\pi} \langle B \rangle \cos n\omega t \, \mathrm{d}\omega t, \tag{5.22}$$

$$\mu_n'' = \frac{1}{\pi h_0} \int_{-\pi}^{\pi} \langle B \rangle \sin n\omega t \, \mathrm{d}\omega t, \tag{5.23}$$

where $\mu_n'$ and $\mu_n''$ are the real and imaginary parts of the harmonic AC permeability, respectively, and there is a relationship between them:

$$\theta_n = \tan^{-1}\left(\frac{\mu_n''}{\mu_n'}\right). \tag{5.24}$$

In the following $\mu_3$ will be calculated assuming the Bean-London model. When $h_0 < H_p = J_c d$, the magnetic flux distribution varies as shown in Fig. 5.11(a) and (b) with phases of $-\pi \le \omega t < 0$ and $0 \le \omega t < \pi$, respectively, and the spatial average of the magnetic flux density is

$$\begin{aligned} \langle B \rangle &= \text{const.} + \frac{\mu_0 h_0^2}{4 J_c d}(1 + \cos \omega t)^2; \quad -\pi \le \omega t < 0, \\ &= \text{const.} + \frac{\mu_0 h_0^2}{4 J_c d}\left[4 - (1 - \cos \omega t)^2\right]; \quad 0 \le \omega t < \pi, \end{aligned} \tag{5.25}$$

where const. $= \mu_0(H_e - h_0) + \mu_0 J_c d/2$. Substituting this into (5.22) and (5.23), a simple calculation gives $\mu_3' = 0$ and

$$\mu_3 = -\mu_3'' = \frac{2\mu_0 h_0}{15\pi J_c d}. \tag{5.26}$$

Hence, $J_c$ can be estimated from the measurement of $\mu_3$. However, note that the above result is correct only when $h_0$ is smaller than the penetration field $H_p = J_c d$.

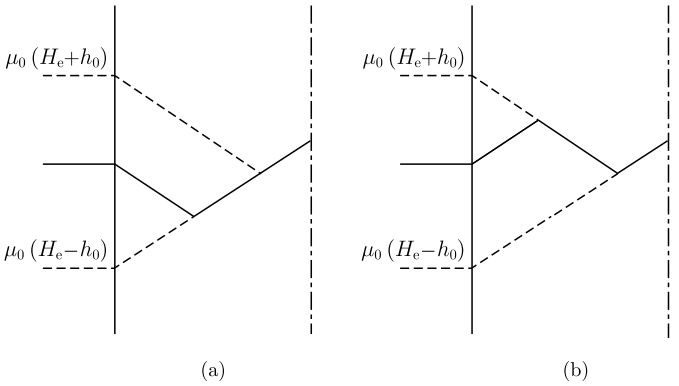


**Fig. 5.11** Magnetic flux distribution in a superconducting slab of thickness $2d$ in a parallel AC magnetic field during processes of (**a**) increasing and (**b**) decreasing field. The Bean-London model is assumed

When $h_0$ is larger than $H_p$, the expression of $\mu_3$ is complicated (see Exercise 5.4). In addition, correct results can be obtained only when the critical state model holds. Equation (5.26) does not hold when the effect of reversible flux motion dominates.

A method to estimate the critical current density of a superconducting thin film involves measuring an induced third harmonic voltage in a coil placed near the film surface which applies an AC magnetic field to the film [11]. In this case the coil axis is perpendicular to the film surface. However, the magnetic field is almost parallel to the film surface due to the shielding current flowing in the film. For a parallel AC magnetic field applied to the surface of a wide superconducting thin film, the third harmonic voltage induced in the coil can be simply calculated using the critical state model. In some experiments a DC magnetic field is superimposed on the superconducting thin film. The DC field only influences the value of the critical current density, but does not influence the third harmonic voltage, since a simple principle of superposition holds in electromagnetism.

It is assumed that a wide superconducting thin film occupies $0 \leq x \leq d$ and an AC magnetic field, $h_0 \cos \omega t$, due to an AC current is applied parallel to the surface of $x = 0$. It is also assumed that the film thickness $d$ is so small in comparison with the coil size that the thickness can be neglected in a calculation of the induced voltage in the coil.

In the case of $h_0 < J_c d$, the magnetic field at the opposite surface, $H(d)$, is zero. Hence, the current induced in a unit length of thin film along the direction of magnetic field is:

$$I'(t) = H(0) - H(d) = h_0 \cos \omega t. \tag{5.27}$$

The corresponding voltage induced in the coil is:

$$V(t) = -K \frac{\mathrm{d}I'(t)}{\mathrm{d}t} = K h_0 \omega \sin \omega t, \tag{5.28}$$

where $K$ is a coefficient determined by the coil. The third harmonic voltage is estimated as

$$V_3 = \left(f_1^2 + f_2^2\right)^{1/2}, \tag{5.29}$$

where $f_1$ and $f_2$ are given by

$$f_1 = \frac{1}{2\pi}\int_0^{2\pi} V(t)\cos 3\omega t \mathrm{d}\omega t, \tag{5.30}$$

$$f_2 = \frac{1}{2\pi}\int_0^{2\pi} V(t)\sin 3\omega t \mathrm{d}\omega t. \tag{5.31}$$

In this case

$$V_3 = 0 \tag{5.32}$$

is easily derived.

In the case of $h_0 \geq J_c d$, we have

$$\begin{aligned} I'(t) &= J_c d - h_0(1-\cos\omega t); \quad 0 \leq \omega t < \theta_0 \\ &= -J_c d; \quad \theta_0 \leq \omega t < \pi, \end{aligned} \tag{5.33}$$

where $\theta_0$ is given by

$$\theta_0 = \cos^{-1}\left(1 - \frac{2J_c d}{h_0}\right). \tag{5.34}$$

This leads to

$$\begin{aligned} V(t) &= -Kh_0\omega\sin\omega t; \quad 0 \leq \omega t < \theta_0 \\ &= 0; \quad \theta_0 \leq \omega t < \pi. \end{aligned} \tag{5.35}$$

Similar results are obtained for the latter half period, $\pi \leq \omega t < 2\pi$. After a simple calculation we have

$$\begin{aligned} f_1 &= 2Kh_0\omega\int_0^{\theta_0}\sin\omega t\cos 3\omega t \mathrm{d}\omega t \\ &= 4Kh_0\omega h_\mathrm{p}(1-h_\mathrm{p})\left(1-8h_\mathrm{p}+8h_\mathrm{p}^2\right) \end{aligned} \tag{5.36}$$

and

$$\begin{aligned} f_2 &= 2Kh_0\omega\int_0^{\theta_0}\sin\omega t\sin 3\omega t \mathrm{d}\omega t \\ &= 8Kh_0\omega\sin\theta_0 h_\mathrm{p}(1-h_\mathrm{p})(1-2h_\mathrm{p}) \end{aligned} \tag{5.37}$$

with

$$h_\mathrm{p} = \frac{J_c d}{h_0} \tag{5.38}$$

and

$$\sin\theta_0 = 2\left(h_\mathrm{p} - h_\mathrm{p}^2\right)^{1/2}. \tag{5.39}$$

Thus, we obtain

$$V_3 = 4K\omega J_\mathrm{c} d\left(1 - \frac{J_\mathrm{c} d}{h_0}\right). \tag{5.40}$$

Hence, if $h_\mathrm{c}$ is the AC magnetic field amplitude at which the third harmonic voltage starts to appear, the critical current density of the film is estimated as

$$J_\mathrm{c} = \frac{h_\mathrm{c}}{d}. \tag{5.41}$$

It should be noted, however, that this estimation is not correct, unless the film thickness is so much thicker than Campbell's AC penetration depth, given by (3.93), that the effect of reversible flux motion can be neglected. In practice, $\lambda_0'$ is estimated as 0.8 μm for the case of $J_\mathrm{c} = 1.0 \times 10^{10}$ A/m$^2$ at $B = 1$ T, where (3.95) is used for $\alpha_\mathrm{L}$ in (3.93) and the relationship $d_\mathrm{i} = 2\pi a_\mathrm{f}$ for point-like defects is assumed. For ordinary thin films thinner than 1 μm, therefore, the measurement of the third harmonic voltage may not give a correct estimation of $J_\mathrm{c}$ in a DC magnetic field but may lead to an overestimation due to the effect of reversible flux motion [12], similarly to other AC measurements. The factor of overestimation is of the order of $\lambda_0'/d$, [12] and is smaller than those involved in Campbell's method (see Exercise 5.3) and AC susceptibility measurements. In the absence of a DC magnetic field, $\lambda_0'$ is expected to be significantly smaller than the above estimation, and this method may be useful for the estimation of $J_\mathrm{c}$ even for fairly thin superconductors.

### 5.4.2 AC Susceptibility Measurement

The critical current density can also be estimated from a measurement of the AC susceptibility. If the magnetization of a superconducting specimen in an AC magnetic field $h_0 \cos\omega t$ is expressed as

$$M(t) = h_0 \sum_{n=0}^{\infty} \left(\chi_n' \cos n\omega t + \chi_n'' \sin n\omega t\right), \tag{5.42}$$

$\chi_n'$ and $\chi_n''$ $(n \geq 1)$ are the real and imaginary parts of the $n$-th AC susceptibility. In terms of $M(t)$, these parts are given by

$$\chi_n' = \frac{1}{\pi h_0} \int_{-\pi}^{\pi} M \cos n\omega t \, \mathrm{d}\omega t, \tag{5.43}$$

$$\chi_n'' = \frac{1}{\pi h_0} \int_{-\pi}^{\pi} M \sin n\omega t \, \mathrm{d}\omega t. \tag{5.44}$$

These quantities are related to the AC permeabilities given by (5.22) and (5.23) as

$$\chi_1' = \frac{\mu_1'}{\mu_0} - 1, \qquad \chi_n' = \frac{\mu_n'}{\mu_0} \quad (n \geq 2) \tag{5.45}$$

with

$$\chi_n'' = \frac{\mu_n''}{\mu_0} \quad (n \geq 1). \tag{5.46}$$

These relationships are easily derived from $M = \langle B \rangle/\mu_0 - (H_e + h_0 \cos \omega t)$. Here, assume again a wide superconducting slab of thickness $2d$, in which the Bean-London model holds. Then, $\chi_1'$ and $\chi_1''$ can be calculated easily:

$$\chi_1' = -1 + \frac{h_0}{2H_p}; \quad h_0 \leq H_p, \tag{5.47a}$$

$$= -\frac{1}{\pi}\left(1 - \frac{h_0}{2H_p}\right)\cos^{-1}\left(1 - \frac{2H_p}{h_0}\right) - \frac{1}{\pi}\left[1 - \frac{4H_p}{3h_0} + \frac{4}{3}\left(\frac{H_p}{h_0}\right)^2\right]\left(\frac{h_0}{H_p} - 1\right)^{1/2}; \quad h_0 > H_p, \tag{5.47b}$$

$$\chi_1'' = \frac{2h_0}{3\pi H_p}; \quad h_0 \leq H_p, \tag{5.48a}$$

$$= \frac{2H_p}{\pi h_0}\left(1 - \frac{2H_p}{3h_0}\right); \quad h_0 > H_p. \tag{5.48b}$$

The dependencies of $\chi_1'$ and $\chi_1''$ on the AC field amplitude are shown in Fig. 5.12(a) and (b), respectively. $\chi_1'$ changes from $-1$ with increasing $h_0$, takes on a value $-1/2$ at $h_0 = H_p$, and then approaches 0 asymptotically. On the other hand, $\chi_1''$ takes on a maximum value $3/4\pi$ at $h_0 = (4/3)H_p \equiv h_m$. Hence, if $h_m$ is obtained from measurements, the critical current density can be estimated as

$$J_c = \frac{3h_m}{4d}. \tag{5.49}$$

In most experiments, $\chi_1''$ is measured under a variation of temperature with a constant amplitude $h_0$. Even in this case, the critical current density is estimated from $J_c = 3h_0/4d$ at the temperature at which $\chi_1''$ takes on a peak value. More exactly speaking, however, the quantity obtained is nothing else besides the temperature at which $J_c$ takes on some given value, since $h_0$ and $d$ are given in such experiments. A common purpose is to know $J_c$ under the desired condition of temperature and magnetic field. In the latter case it is required to measure $\chi_1''$ as a function of $h_0$ at the given temperature and magnetic field, as shown in (5.48a) and (5.48b).

$\chi_1''$ is equal to $\mu_1''/\mu_0$ and is directly related to the energy loss density as shown in (3.102). When the size of the superconducting specimen is comparable to or smaller

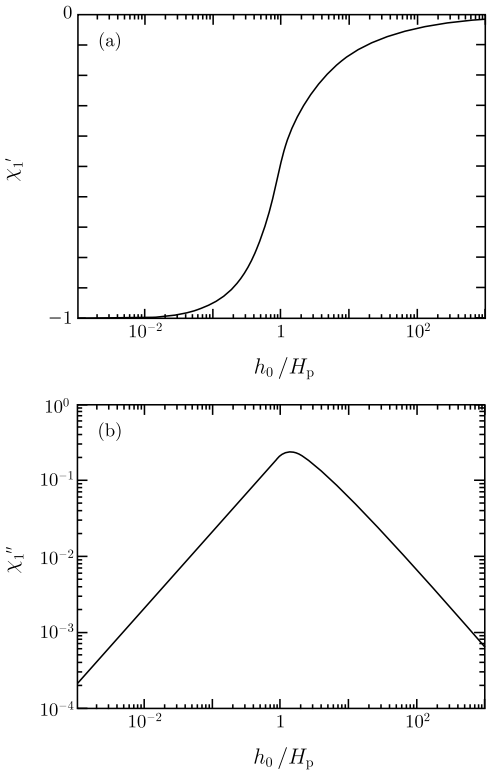


**Fig. 5.12** Prediction of the Bean-London model on the AC susceptibility of a superconducting slab in a parallel AC magnetic field: (**a**) real part and (**b**) imaginary part

than Campbell's AC penetration depth $\lambda_0'$, the critical state model does not hold due to the reversible flux motion, as discussed in Sect. 3.7. In this case the Campbell model [8] is useful for analyzing the magnetic flux distribution, and the distribution can be derived by solving (3.97) numerically. Then, the magnetization $M$ is obtained from the distribution, and $\chi_1'$ and $\chi_1''$ are derived from (5.43) and (5.44). The results obtained in this manner [13] are shown in Figs. 5.13 and 5.14. Figure 5.13 shows the results for $d/\lambda_0' = 10$, which corresponds to the case where the critical state model describes the magnetic behavior correctly. In fact, this result can be approximately explained by the critical state model.

By contrast, Fig. 5.14 shows the case of $d/\lambda_0' = 0.3$ where the effect of reversible flux motion is expected to be pronounced. In fact, $\chi_1'$ deviates significantly from the predicted value of $-1$ of the critical state model in the region of small amplitude, showing an extremely small shielding effect. The maximum value of $\chi_1''$ is also much smaller than predicted by the critical state model with a considerable shift of the position of the maximum to a higher AC field amplitude. Thus, the value of the critical current density obtained by substitution of the observed $h_m$ into (5.49) is considerably overestimated. In Fig. 5.14, for example, the critical current density is overestimated by a factor of about 30. Hence, it is required to judge correctly if the analysis using (5.49) is suitable for a superconductor of a relatively small size. For

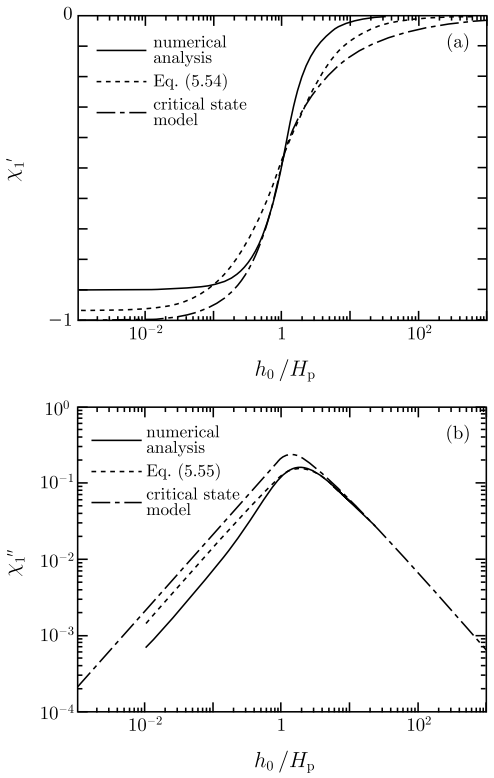


**Fig. 5.13** (**a**) Real and (**b**) imaginary parts of the AC susceptibility of a superconducting slab for $d/\lambda_0' = 10$. The *solid lines* show the results of the numerical analysis of (3.97) based on the Campbell model, and the *chained lines* show the results of the Bean-London model. The *broken lines* represent the approximate formulae given by (5.54) and (5.55). All give similar results

this purpose, it is useful to compare the maximum value of $\chi_1''$, denoted by $\chi_m''$, with the theoretically predicted value $3/4\pi$. That is, if $\chi_m''$ is comparable to the predicted value, (5.49) is applicable, and if $\chi_m''$ is much smaller than the predicted value, the use of (5.49) may lead to a serious overestimation. There have been many reports on high-temperature superconductors indicating that $\chi_m''$ becomes smaller as the temperature is raised to the critical temperature. This is believed to originate from the reversible flux motion. Note that Campbell's AC penetration depth $\lambda_0'$ takes on a larger value for a superconductor with a weaker pinning force. In high-temperature superconductors the pinning force is originally weak and becomes even weaker at a higher temperature, resulting in very large $\lambda_0'$. Hence, this reversible behavior can occur even in relatively large specimens.

To analyze the behavior under a reversible flux motion, it is required to solve numerically (3.97), which is a nonlinear differential equation. However, this is not simple. Hence, approximate formulae for AC susceptibilities are proposed here, since the dependencies of these formulae on the AC field amplitude are rather simple, as shown in Figs. 5.13 and 5.14. One of the conditions to be satisfied is that the result should approach the prediction of the critical state model, (5.47a), (5.47b), (5.48a) and (5.48b), in the irreversible limit. Characteristic points for $\chi_1'$ are: $\chi_1' \to -1$ for $h_0 \ll H_p$, $\chi_1' = -1/2$ at $h_0 = H_p$ and $\chi_1 \to 0$ for $h_0 \gg H_p$. Characteristic points for

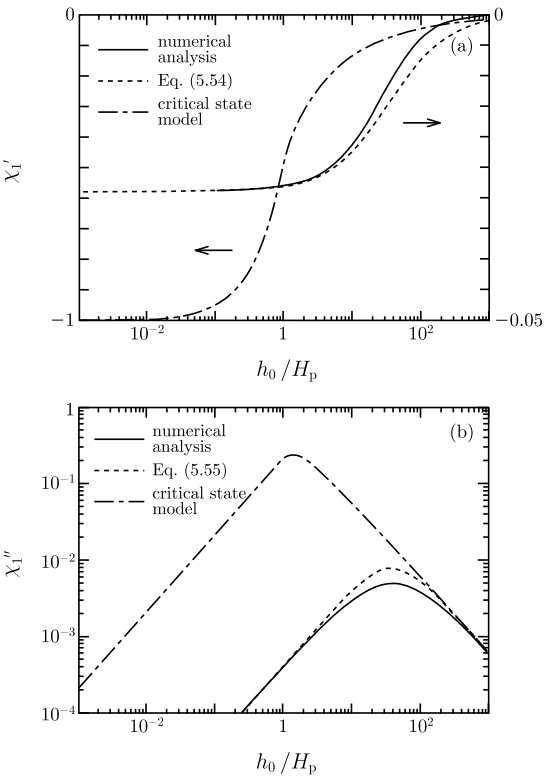


**Fig. 5.14** (**a**) Real and (**b**) imaginary parts of the AC susceptibility of a superconducting slab for $d/\lambda_0' = 0.3$. The *solid*, *chained* and *broken lines* show the results of the numerical analysis of (3.97), the results of the critical state model and the approximate formulae, respectively. The results of the critical state model deviate greatly from the other two

$\chi_1''$ are that it approaches (5.48a) for $h_0 \ll H_p$ and $\chi_1'' \to 2H_p/\pi h_0$ for $h_0 \gg H_p$. Candidates which satisfy the above requirements are

$$\chi_1' = -\frac{H_p}{H_p + h_0}, \tag{5.50}$$

$$\chi_1'' = \frac{2}{\pi} \cdot \frac{H_p h_0}{3H_p^2 + h_0^2}. \tag{5.51}$$

$h_m = \sqrt{3}H_p$ and $\chi_m'' = 1/\sqrt{3}\pi \simeq 0.184$ are obtained from (5.51), while $h_m = (4/3)H_p$ and $\chi_m'' = 3/4\pi \simeq 0.239$ are obtained from (5.48b) based on the critical state model. Thus, these results are not very different from each other.

In the limit of reversible flux motion, where $d$ is sufficiently smaller than $\lambda_0'$ and $h_0$ is sufficiently small, a simple calculation shows that $\chi_1'$ approaches asymptotically

$$\chi_1' = -1 + \frac{\lambda_0'}{d}\tanh\left(\frac{d}{\lambda_0'}\right) \simeq -\frac{1}{3}\left(\frac{d}{\lambda_0'}\right)^2. \tag{5.52}$$

On the other hand, $\chi_1''$ approaches

$$\chi_1'' = \frac{h_0}{6\pi H_p}\left(\frac{d}{\lambda_0'}\right)^4. \tag{5.53}$$

In the above equations (3.102), (3.110) and (5.46) were used with replacement of $d_f$ by $2d$. When $h_0$ is sufficiently larger than $H_p$ given by (3.111), the behavior becomes irreversible even if $d$ is smaller than $\lambda_0'$, and $\chi_1'$ and $\chi_1''$ approach 0 and $2H_p/\pi h_0$, respectively.

Here approximate formulae are proposed [13]:

$$\chi_1' = -\frac{H_p}{[1+3(\lambda_0'/d)^2]H_p + h_0}, \tag{5.54}$$

$$\chi_1'' = \frac{2}{\pi}\cdot\frac{H_p h_0}{3[1+2(\lambda_0'/d)^2]^2 H_p^2 + h_0^2}. \tag{5.55}$$

These satisfy the above requirements. Figures 5.13 and 5.14 show a comparison between these formulae and the results of numerical calculation. It is found that a fairly good agreement is obtained in both limits of $d \gg \lambda_0'$ and $d \ll \lambda_0'$. The important results of these formulae are as follows: firstly, $\chi_1'$ does not reach $-1$ even at very low temperature, when the sample size is smaller than $\lambda_0'$. Hence, it is not correct to evaluate a superconducting volume fraction from this value of $\chi_1'$. This is similar to the incorrect estimation of the superconducting volume fraction from DC susceptibility, as described in Sect. 3.6. Secondly, it is found from (5.55) that the AC field amplitude at which $\chi_1''$ peaks is

$$h_m = \sqrt{3}\left[1+2\left(\frac{\lambda_0'}{d}\right)^2\right]H_p \tag{5.56}$$

and the peak value is

$$\chi_m'' = \frac{1}{\sqrt{3}\pi[1+2(\lambda_0'/d)^2]}. \tag{5.57}$$

Hence, $J_c$ cannot be estimated only from $h_m$. This is because the value of $\lambda_0'$ is unknown. However, (5.56) and (5.57) allow us to derive

$$h_m\chi_m'' = \frac{H_p}{\pi} = \frac{J_c d}{\pi}. \tag{5.58}$$

Thus, the unknown quantity $\lambda_0'$ is eliminated and $J_c$ can be obtained from the value of the product. From this $J_c$ value $\lambda_0'$ can be determined. The value of $\lambda_0'$ can also be obtained by comparing the slope of the observed minor curve of the DC magnetization with (3.112) in which $d_f$ is replaced by $2d$.

When the size of the superconducting sample is much larger than $\lambda_0'$, the critical state model holds. Even in this case (5.58) from which $J_c$ can be determined still holds. However, the further analysis to estimate $\lambda_0'$ may contain a large error.

## 5.5 Exercises

5.1 Assume that an AC magnetic field of amplitude $h_0$ is applied parallel to a superconducting slab $2d$ in thickness and $w$ in width ($w \gg 2d$). When the Bean-London model holds in the superconducting slab, show that the penetration depth of the AC field is given by $\lambda' = h_0/J_c$, and that the $h_0$ vs. $\lambda'$ curve represents the magnetic flux distribution for $h_0 < H_p = J_c d$, using the analysis based on Campbell's method. Show also that $\lambda' = d$ for $h_0 > H_p$.

5.2 Estimate the error of the critical current density derived from the modified Campbell's method, when the amplitude $\Phi$ of the AC magnetic flux moving into and out of the superconducting specimen is replaced by the amplitude of the component of fundamental frequency $\Phi'$. Assume that the Bean-London model holds for the magnetic flux distribution.

5.3 Calculate the apparent value of the penetration depth $\lambda'$ of an AC magnetic field for a superconducting specimen of a size smaller than Campbell's AC penetration depth $\lambda'_0$, and discuss the reason why the critical current density cannot be estimated correctly using the analysis based on Campbell's method.

5.4 Calculate $\mu_3$ when the amplitude of the AC magnetic field $h_0$ is larger than the penetration field $H_p = J_c d$.

5.5 Derive (5.47a), (5.47b), (5.48a) and (5.48b).

## References


1. T. Matsushita, Y. Himeda, M. Kiuchi, J. Fujikami, K. Hayashi, IEEE Trans. Appl. Supercond. **15**, 2518 (2005)
2. A.M. Campbell, J. Phys. C **2**, 1492 (1969)
3. T. Matsushita, T. Honda, K. Yamafuji, Mem. Fac. Eng., Kyushu Univ. **43**, 233 (1983)
4. T. Matsushita, T. Tanaka, K. Yamafuji, J. Phys. Soc. Jpn. **46**, 756 (1979)
5. R.W. Rollins, H. Küpfer, W. Gey, J. Appl. Phys. **45**, 5392 (1974)
6. T. Matsushita, T. Honda, Y. Hasegawa, Y. Monju, J. Appl. Phys. **54**, 6526 (1983)
7. B. Ni, T. Munakata, T. Matsushita, M. Iwakuma, K. Funaki, M. Takeo, K. Yamafuji, Jpn. J. Appl. Phys. **27**, 1658 (1988)
8. A.M. Campbell, J. Phys. C **4**, 3186 (1971)
9. A. Kikitsu, Y. Hasegawa, T. Matsushita, Jpn. J. Appl. Phys. **25**, 32 (1986)
10. C.P. Bean, Rev. Mod. Phys. **36**, 31 (1964)
11. H. Yamasaki, Y. Mawatari, Y. Nakagawa, Appl. Phys. Lett. **82**, 3275 (2003)
12. Y. Fukumoto, T. Matsushita, Supercond. Sci. Technol. **18**, 861 (2005)
13. T. Matsushita, E.S. Otabe, B. Ni, Physica C **182**, 95 (1991)